Asymmetric Capacitor-Loaded Marchand Balun-Based Four-Stacked Power Amplifier Utilized *C*-Band Stimulus Source in SOI CMOS

Seongwoog Oh, *Member, IEEE*, and Jungsuek Oh, *Senior Member, IEEE*

***Abstract*— This letter presents a novel stimulation source with a four-stack power amplifier (PA) based on an asymmetric capacitor-loaded Marchand balun. The stimulus source comprises a cross-coupled voltage-controlled oscillator (VCO), common-source buffer, and two-stage four-stacked PA. The target power level of the PA was specified by performing an analysis assuming a realistic far-field stimulation environment. Loading two capacitors with different capacitances onto the OFF-chip Marchand balun eliminates the imbalance between the two balun nodes. Improvements in magnitude and phase balance show an enhanced performance and are also robust against fabrication errors. A stimulus source was designed and fabricated at 6.5 GHz using 0.28-μm silicon on insulator complementary metal–oxide–semiconductor (CMOS) process for validation. The measured maximum output power and peak drain efficiency (DE) were 33.4 dBm and 28.3%, respectively. The proposed stimulus source is the first-of-a-kind system with a watt-level output for behavioral experiments in the *C*-band.**

***Index Terms*— High-power power amplifier (PA), microwave, monolithic microwave integrated circuit, stimulation.**

I. Introduction

MICROWAVE frequencies, which are widely used for communication and sensing, are now expanding into bioapplications. Several recent studies simulated various biological tissues using modulated microwave signals [1], [2], [3], [4]. The existing stimulation techniques mainly assume an environment in which a structure, such as a probe, is directly in contact with a bio-tissue. The direct method has an advantage in terms of efficiency but experiences critical issues of heat transfer from the stimulus source and heavy RF cable weight. These limitations make it challenging to test the effect of microwave stimulation only in animal experiments; therefore, the need for a far-field stimulation method is emerging.

Among the voltage-controlled oscillator (VCO), buffer, and power amplifier (PA) constituting the stimulus source, it is necessary to maximize the PA output power to support far-field stimulation. Therefore, several topologies have been proposed for achieving high output while maintaining the high efficiency of complementary metal–oxide–semiconductor (CMOS) PA [5], [6].

In the mentioned studies [7], [8], optimizations of load impedance based on common sources were carried out, yet due to the low quality factor of the ON-chip transformer/inductor combined with a low supply voltage, the output power was limited around 20 dBm. While [9], [10] have introduced cascode-based PAs, the realization of watt-level output power is still a significant hurdle. Previous research on four-stacked PAs, which focused on achieving high output power, was directed toward the communication frequency band [11], [12], [13], and reports in the *C*-band are scarce. Moreover, most research into PAs that achieve output power above 2 W has been done with GaN processes, which require high cost and exhibit low integration [14], [15]. We introduce the design and fabrication of a four-stacked PA that incorporates an asymmetric capacitor-loaded Marchand balun for a 6.5-GHz stimulus source.

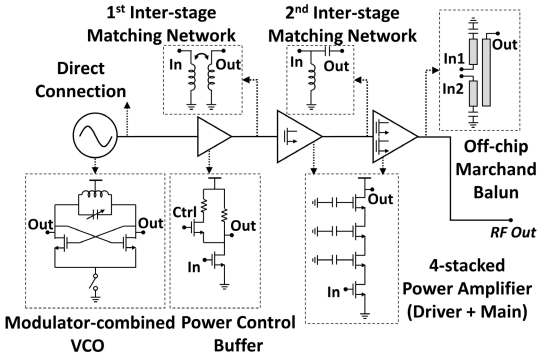

Fig. 1. Block diagram of the proposed stimulus source with a conceptual schematic.

II. System Design

A. Study of RF Stimulus Source

As shown in Fig. 1, the proposed stimulus source consists of a VCO coupled with a modulator, a buffer with a variable resistor as a load, and two-stage four-stacked PA. The conceptual schematic of each component is shown briefly, except for the VCO and Marchand balun, which are simplified to a single-ended form; however, in the implementation all the components use a differential-type topology. The VCO and the buffer were directly connected. The buffer and first

Manuscript received 14 November 2023; accepted 2 December 2023. Date of publication 2 February 2024; date of current version 13 March 2024. This work was supported by Samsung Electronics Company Ltd. *(Corresponding author: Jungsuek Oh.)*

Seongwoog Oh was with the Department of Electrical and Computer Engineering (ECE), Institute of New Media and Communications (INMC), Seoul National University, Seoul 151-742, Republic of Korea. He is now with the Department of Electrical and Computer Engineering, University of California San Diego, La Jolla, CA 92093 USA.

Jungsuek Oh is with the Department of Electrical and Computer Engineering (ECE), Institute of New Media and Communications (INMC), Seoul National University, Seoul 151-742, Republic of Korea (e-mail: jungsuek@snu.ac.kr).

Color versions of one or more figures in this letter are available at https://doi.org/10.1109/LMWT.2023.3348162.

Digital Object Identifier 10.1109/LMWT.2023.3348162

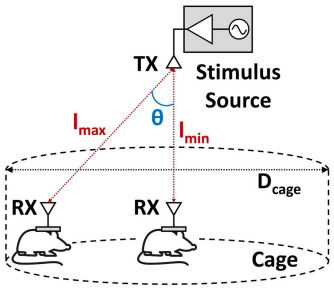

Fig. 2. Behavioral experimental scenario with a far-field stimulus consisting of a stimulus source and TX/RX antenna.

TABLE I
STIMULUS ENVIRONMENT/COMPONENT PARAMETERS

Parameter	Value	Topology
λ	46.12 mm	Wavelength at 6.5 GHz
G_{RX0}	7 dBi	Single patch antenna
G_{TX0}	13 dBi	2 × 2 patch antenna array
D_{cage}	60 cm	Mouse cage for behavior experiment

stage of the PA, which is the driver amplifier, are matched using a transformer. The inter-stage matching network (IMN) of the two-stage PA comprises a high-pass filter-type matching network. Finally, a Marchand balun is used for output matching and transforms the differential output of the main amplifier into the single-ended signal required for antenna connection.

As shown in Fig. 2, for the experimental behavioral scenario, the power received by the target changes with the distance between the fixed transmit (TX) antenna and the moving receive (RX) antenna. Therefore, the source integrated circuit must adjust the output power, P_t, with constraints based on the Friis transmission formula

$$P_t + G_{\mathrm{RX}}(\theta) + G_{\mathrm{TX}}(\theta) + 20\log\left(\frac{\lambda}{4\pi l_{\max}}\right) < P_r < P_t + G_{\mathrm{RX0}} + G_{\mathrm{TX0}} + 20\log\left(\frac{\lambda}{4\pi l_{\min}}\right) \quad (1)$$

where λ is the wavelength corresponding to the carrier frequency, P_r is the power received by the test subject, and G_{RX} and G_{TX} are the gains of the RX and TX antennas, respectively, according to the angle θ. For a cage diameter D_{cage}, $l_{\min}$ and $l_{\max}$ represent the minimum and maximum distances between the TX and RX antenna, respectively. Practically, to minimize the effect of weight on the subject, an antenna configuration that can achieve a weight of 4 g or less is required [16]; therefore, the RX antenna uses a simple structure, such as a patch antenna.

To derive P_t and the power control range, ΔP_t, of the stimulus source, a hypothetical system configuration was created [17], [18], [19], as shown in Table I. The RX antenna uses a single patch to minimize the weight, and the TX uses a patch array structure to improve the gain. Because increasing the antenna gain to mitigate the maximum P_t reduces the half-power beamwidth, the TX antenna is compromised to a 2 × 2 patch array. Considering the far-field distance by the frequency-dependent antenna and the diameter of the cage in which the subject moves, $l_{\min}$ and $l_{\max}$ are 43.4 and 52.8 cm, respectively, with $\theta = 34.7°$. Based on previous studies [4],

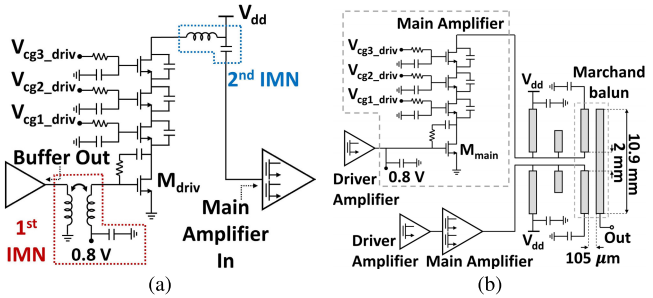

Fig. 3. Schematic of the (a) driver and (b) main amplifier with inter-stage/Marchand balun-based matching networks.

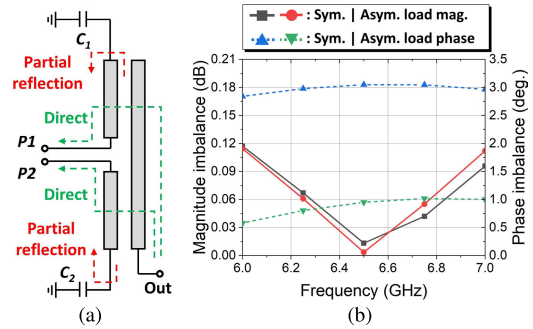

Fig. 4. (a) Couplings in asymmetric capacitor-loaded Marchand balun. (b) Magnitude/phase balance between input nodes with respect to frequency.

[20], [21], the required P_r of 9 dBm is established, and the values obtained above are reflected in (1); the maximum P_t and ΔP_t are 32.2 dBm and 3 dB, respectively. Therefore, the buffer is designed to control the output power of 3 dB to compensate for the subject location change and enable constant power delivery and the oscillator must be capable of generating C-band signal covering 6.5 GHz. Based on the analysis, considering the constraints and practical conditions, the PA technique for high power is required to meet the watt-level output power.

B. Design of Four-Stacked PA

A high supply voltage must be used through stacking transistors to obtain more than 32.2 dBm of power with the CMOS process. In this study, a drain voltage of 8 V was carefully chosen, and four transistors were stacked considering the individual transistor shows 2.75-V drain/gate breakdown voltage. The gate voltages of the four-stacked cell transistors are 0.8, 2.8, 4.8, and 6.8 V from the bottom, respectively. Because there are no back-via holes in the CMOS process, both the driver and main amplifier comprising the PA are used in a differential structure to suppress the degeneration effect caused by the parasitic inductor due to wedge bonding. Fig. 3 shows the four-stacked transistor cell of the driver and the main amplifier with IMNs. The first IMN comprises an integrated transformer such that the output of the buffer and the input of the driver amplifier are matched while biasing the gate. The second IMN achieves matching and bias isolation between the drain and gate through a series inductor and capacitor, respectively.

Fig. 4(a) shows a schematic of the proposed asymmetric capacitor-loaded Marchand balun. For practical Marchand balun implementation, there must be a physical distance between the two couplers which causes impedance imbalance

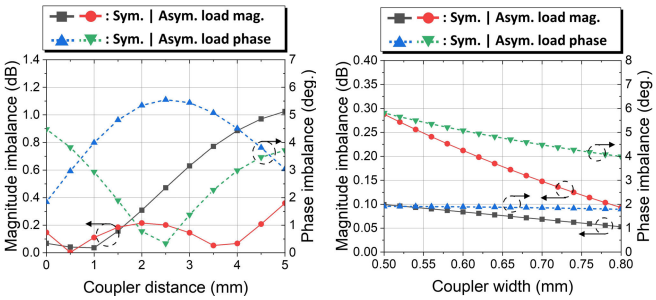

Fig. 5. Magnitude and phase balance comparison with coupler. (a) Distance. (b) Width variation for asymmetric capacitor-loaded and conventional Marchand balun (coupler width = 0.7 mm, distance = 2 mm).

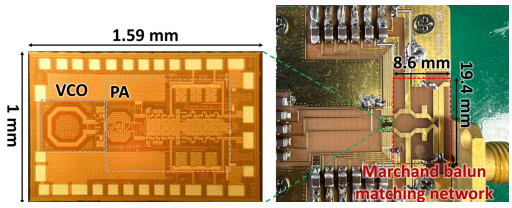

Fig. 6. Photograph of the fabricated stimulus source of integrated circuit and PCB matching circuit.

between $P1$ and $P2$. The reflection was adjusted by optimizing the capacitance of $C1$ to 0.84 $C2$ to improve the impedance balance between the nodes. Fig. 4(b) shows that the proposed method can improve the phase balance between two input balun nodes compared with the conventional configuration of identical RF short-capacitor loading. Through improved impedance asymmetry, the output power and efficiency of the two-stage four-stacked PA increased by up to 33.8 dBm and 29.5%, respectively. Fig. 5(a) shows the result of an imbalance of magnitude and phase between $P1$ and $P2$ nodes according to the coupler distance. A conventional design method was used for the simulation of the symmetric case with 5 pF used to be the ac ground at 6.5 GHz. The proposed asymmetric capacitor-loaded technique shows a degraded phase imbalance for zero-gap or low-gap, which is impractical but achieves a phase and magnitude imbalance of less than 1° and less than 0.2 dB at a manufacturable distance of 2 mm. Finally, with the proposed technique, it was possible to achieve an improvement of 2.6° of phase and 0.1 dB in magnitude balance. Fig. 5(b) also shows the effect of process variations and mismatches on the coupler width. It can be seen that the proposed structure exhibits excellent magnitude and phase imbalance performance while exhibiting a relatively flat change. The insensitivity of the changes in phase and magnitude to the variation in each gap and width shows that it is useful for process and mismatch. The proposed PA, with the improved balance of the differential PA drain impedance, achieved a gain and drain efficiency (DE) improvement of 5.9 dB and 2.2% at 6.5 GHz over the conventional configuration, respectively.

III. Measurement Results

Fig. 6 shows a photograph of the stimulus-source module fabricated to demonstrate the proposed topology. The integrated circuit comprising the VCO and PA is fabricated

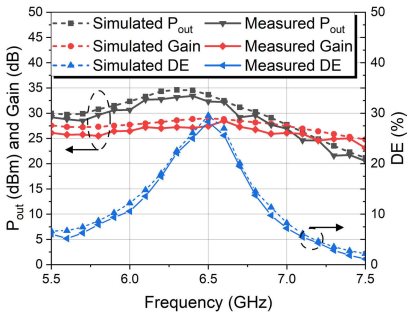

Fig. 7. Comparison of the simulated and measured results of the proposed stimulus source.

TABLE II
Comparison With Recent RF Stimulus Systems

Study (Tx/PAs)	CMOS Process	V_{supply} (V)	Frequency (GHz)	Gain (dB)	P_{out} (dBm)	DE (%)
This Work	0.28-μm*	8	6.5	28.5	33.4†	28.3^{a}
Ref. [7]	0.18-μm	3.3	5-6.5	25-28	21.8†	16.5^{b}
Ref. [8]	0.18-μm	1.9	5.8	>7	19.8‡	28.1
Ref. [9]	0.13-μm	2	5.8	11.5	17.3‡	34.4
Ref. [10]	0.18-μm	1.8	5.8	19.4	19.5	33.5
Ref. [11]	65-nm	3.6	0.9	18	31	62

†: P_{sat}; ‡: P_{1dB}; *: SOI process; ^{a}: Overall system efficiency. ^{b}: Estimated.

in a 0.28-μm SOI CMOS process and occupies an area of 1×1.59 mm^2. The proposed Marchand balun-based output-matching network was fabricated using a conventional printed circuit board (PCB) process with 0.4T FR4 ($\epsilon_r = 4.6$). The Keysight ADS was used for the simulations. The measurements were performed using a Keysight N7080A vector network analyzer, an N8481A power sensor, and an E4417 power meter. Fig. 7 shows the simulation and measured results of the saturated output power, PA gain, and DE of the overall stimulus source. The measured peak DE is 28.7% at 6.5 GHz, and the following output power driven by an internal VCO is 33.4 dBm. The measured gain is calculated considering VCO output power and results in 23.1–28.5 dB across the 5.5–7.5-GHz band. Table II summarizes the measured performance of the source and its comparison with other state-of-the-art works. The proposed work achieved comparable DE with the highest output power and gain among PAs fabricated in other CMOS processes.

IV. Conclusion

This study proposed a novel C-band stimulus source comprising an asymmetric capacitor-loaded Marchand balun, two-stage four-stacked PA, and VCO. The requirements were analyzed based on realistic far-field stimulation environments to articulate the target specifications of the stimulus sources. The impedance balance was improved by loading different capacitors on the Marchand balun used for matching to enhance the PA output and efficiency. The proposed stimulus source can be a solution for the microwave stimulation of C-band frequencies.

Acknowledgment

The EDA tool was supported by the IC Design Education Center (IDEC), South Korea.

REFERENCES

[1] K. Kim, T. Seo, K. Sim, and Y. Kwon, "Magnetic nanoparticle-assisted microwave hyperthermia using an active integrated heat applicator," *IEEE Trans. Microw. Theory Techn.*, vol. 64, no. 7, pp. 2184–2197, Jul. 2016.

[2] M. Bachmann, J. Lass, A. A. Ioannides, and H. Hinrikus, "Brain stimulation by modulated microwave radiation: A feasibility study," in *Proc. EMF-Med 1st World Conf. Biomed. Appl. Electromagn. Fields*, Sep. 2018, pp. 1–2.

[3] A. Madannejad, S. Sadeghi, J. EbrahimiZadeh, F. Ravanbakhsh, M. D. Perez, and R. Augustine, "Microwave beamforming for non-invasive brain stimulation," in *IEEE MTT-S Int. Microw. Symp. Dig.*, Dec. 2020, pp. 1–4.

[4] S. Oh, D. Jung, T. Seo, Y. Huh, J. Cho, and J. Oh, "6.5-GHz brain stimulation system using enhanced probe focusing and switch-driven modulation," *IEEE Trans. Microw. Theory Techn.*, vol. 69, no. 9, pp. 4107–4117, Sep. 2021.

[5] K.-C. Tsai and P. R. Gray, "A 1.9-GHz, 1-W CMOS class-E power amplifier for wireless communications," *IEEE J. Solid-State Circuits*, vol. 34, no. 7, pp. 962–970, Jul. 1999.

[6] M. Fathi, D. K. Su, and B. A. Wooley, "A stacked 6.5-GHz 29.6-dBm power amplifier in standard 65-nm CMOS," in *Proc. IEEE Custom Integr. Circuits Conf.*, Sep. 2010, pp. 1–4.

[7] M. Liu, N. Ding, and Y. Wang, "A C-band CMOS transmitter with a 6-bit phase shifter and power amplifier for phased array systems," in *Proc. 6th Int. Conf. Integr. Circuits Microsyst. (ICICM)*, Oct. 2021, pp. 250–253.

[8] J. Carls, F. Ellinger, R. Eickhoff, P. Sakalas, S. von der Mark, and S. Wehrli, "Design of a C-band CMOS class AB power amplifier for an ultra low supply voltage of 1.9 V," in *IEEE MTT-S Int. Microw. Symp. Dig.*, 2007, pp. 786–789.

[9] Q. Liu, S. Jiangtao, Y. Shu, K. Horie, N. Itoh, and T. Yoshimasu, "A high efficiency and high linearity power amplifier utilizing post-linearization technique for 5.8 GHz DSRC applications," in *Proc. IEEE Topical Conf. Power Modeling Wireless Radio Appl.*, Jan. 2011, pp. 45–48.

[10] R. E. Rad, S. Kim, B. S. Rikan, and K.-Y. Lee, "A high power high efficient 5.8 GHz CMOS class—A power amplifier for a WPT application," in *Proc. 12th Int. Conf. Ubiquitous Future Netw. (ICUFN)*, Aug. 2021, pp. 184–186.

[11] S. Leuschner, S. Pinarello, U. Hodel, J.-E. Mueller, and H. Klar, "A 31-dBm, high ruggedness power amplifier in 65-nm standard CMOS with high-efficiency stacked-cascode stages," in *Proc. IEEE Radio Freq. Integr. Circuits Symp.*, May 2010, pp. 395–398.

[12] V. Diddi, H. Gheidi, J. Buckwalter, and P. Asbeck, "High-power, high-efficiency digital polar Doherty power amplifier for cellular applications in SOI CMOS," in *Proc. IEEE Topical Conf. Power Modeling Wireless Radio Appl. (PAWR)*, Jan. 2016, pp. 18–20.

[13] H. Zhang, K. Xie, and K. Wang, "A Ka-band 4-stack power amplifier in 130-nm SiGe BiCMOS," in *Proc. 13th U.K.-Europe-China Workshop Millimetre-Waves THz Technol. (UCMMT)*, Aug. 2020, pp. 1–3.

[14] H. Xie, Y. J. Cheng, Y. R. Ding, L. Wang, and Y. Fan, "A C-band high-efficiency power amplifier MMIC with second-harmonic control in 0.25 μm GaN HEMT technology," *IEEE Microw. Wireless Compon. Lett.*, vol. 31, no. 12, pp. 1303–1306, Dec. 2021.

[15] W. Shi et al., "Design of a C-band high efficiency power amplifier with compact harmonic control network," *IEEE Microw. Wireless Compon. Lett.*, vol. 31, no. 9, pp. 1059–1062, Sep. 2021.

[16] J. Voigts, J. H. Siegle, D. L. Pritchett, and C. I. Moore, "The FlexDrive: An ultra-light implant for optical control and highly parallel chronic recording of neuronal ensembles in freely moving mice," *Frontiers Syst. Neurosci.*, vol. 7, pp. 1–8, May 2013. [Online]. Available: https://www.frontiersin.org/articles/10.3389/fnsys.2013.00008

[17] T. Mao and M. Zhang, "A low-profile dual-band elliptical patch antenna suitable for WiFi with bandwidth," in *Proc. 13th Int. Symp. Antennas, Propag. EM Theory (ISAPE)*, Dec. 2021, pp. 1–3.

[18] Y. Cheng and Y. Dong, "Wideband circularly polarized split patch antenna loaded with suspended rods," *IEEE Antennas Wireless Propag. Lett.*, vol. 20, no. 2, pp. 229–233, Feb. 2021.

[19] H. Mei, K. A. Thackston, R. A. Bercich, J. G. R. Jefferys, and P. P. Irazoqui, "Cavity resonator wireless power transfer system for freely moving animal experiments," *IEEE Trans. Biomed. Eng.*, vol. 64, no. 4, pp. 775–785, Apr. 2017.

[20] S. Oh and J. Oh, "Novel heat-mitigating chip-on-probe for brain stimulation behavior experiments," *Sensors*, vol. 20, no. 24, p. 7334, Dec. 2020. [Online]. Available: https://www.mdpi.com/1424-8220/20/24/7334

[21] Y. Tufail et al., "Transcranial pulsed ultrasound stimulates intact brain circuits," *Neuron*, vol. 66, no. 5, pp. 681–694, Jun. 2010.